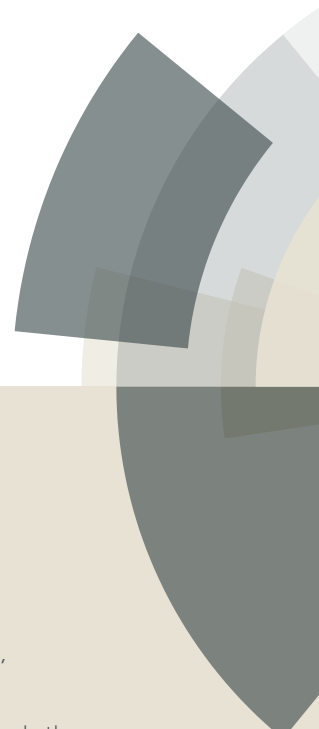


This is an Accepted Manuscript of the following article: *Phys. Chem. Chem. Phys.*, 2017, 19, 25691-25696.

The final publication is available at © Royal Society of Chemistry  
<https://doi.org/10.1039/C7CP04975G>

# PCCP

Accepted Manuscript



This article can be cited before page numbers have been issued, to do this please use: J. A. Avila-Niño, M. Reyes-Reyes and R. López-Sandoval, *Phys. Chem. Chem. Phys.*, 2017, DOI: 10.1039/C7CP04975G.



This is an Accepted Manuscript, which has been through the Royal Society of Chemistry peer review process and has been accepted for publication.

Accepted Manuscripts are published online shortly after acceptance, before technical editing, formatting and proof reading. Using this free service, authors can make their results available to the community, in citable form, before we publish the edited article. We will replace this Accepted Manuscript with the edited and formatted Advance Article as soon as it is available.

You can find more information about Accepted Manuscripts in the [author guidelines](#).

Please note that technical editing may introduce minor changes to the text and/or graphics, which may alter content. The journal's standard [Terms & Conditions](#) and the ethical guidelines, outlined in our [author and reviewer resource centre](#), still apply. In no event shall the Royal Society of Chemistry be held responsible for any errors or omissions in this Accepted Manuscript or any consequences arising from the use of any information it contains.



PCCP

ARTICLE

## Study of the presence of spherical deformations on the Al top electrode due to electroforming in rewritable organic resistive memories

J.A. Ávila-Niño,<sup>a</sup> M. Reyes-Reyes<sup>b\*</sup> and R. López-Sandoval<sup>a\*</sup>

Received 00th January 20xx,  
Accepted 00th January 20xx

DOI: 10.1039/x0xx00000x

www.rsc.org/

Physical deformations are observed at the top electrodes during the electroforming process in Al/PEDOT:PSS+nitrogen doped multiwalled carbon nanotubes (N-MWCNTs)/Al rewritable resistive memory devices. These physical deformations arise from electrochemical reactions, i.e., a reduction reaction in the native Al oxide layer, which is similar to those reported in TiO<sub>2</sub>-based resistive memory devices. These memory devices are electroformed at the ON state using an ~2 V pulse or at the OFF state using an ~3 V pulse. These processes are current-controlled; a minimum compliance current is necessary to obtain the electroforming of the device, generally between 5 to 10 mA. SEM and AFM micrographs show the presence of spherical deformations at the top electrode due to O<sub>2</sub> gas formation generated by the reduction in the native AlOx layer during the electroformation, with a diameter of ~7 micrometres for positive voltage or a smaller diameter of ~3 micrometres for negative voltage. After top-electrode delamination, circular craters are found in the active layer in the vicinity of N-MWCNTs, which only occurs when a negative voltage is used in the electroformation, indicating that film damage is induced by oxygen bubbles created at the bottom electrode/polymeric film interface.

(positive voltage), some of this O<sub>2</sub> gas can escape from the device,

### A. Introduction

Bipolar rewritable memory devices can be switched between two different resistive states due to the application of different voltage polarities.<sup>1</sup> Resistive switching has been studied since the early 1960s in metal-insulator-metal (MIM) memories in Al<sub>2</sub>O<sub>3</sub> films<sup>2</sup> and in other oxide films<sup>3,4</sup>, some of them spontaneously generated during the device fabrication<sup>5-7</sup> as well as in organic layers.<sup>8,9</sup> Among the different mechanisms proposed to explain the switching effect, the filamentary creation and motion of oxygen vacancies are the two principal mechanisms proposed in the literature.<sup>1</sup> It has been reported that the creation of oxygen vacancies during the electroforming process in memory devices is accompanied by physical deformation on the top electrode.<sup>10,11</sup> These phenomena have been extensively studied by the Williams group<sup>12,13</sup> in Pt/TiO<sub>2</sub>/Pt rewritable memory devices. They proposed that oxygen vacancy migration in the oxide layer (50 nm), which forms conducting filaments connecting both electrodes, is the mechanism of the resistive switching. These Pt/TiO<sub>2</sub>/Pt devices showed micron-size protrusions at the oxide/top electrode interface for positive and negative voltages applied to the top electrode due to O<sup>2-</sup> drift towards the anode, where these oxygen anions evolve to oxygen gas. When the oxygen gas bubbles are created at the top interface

whereas when they are created at the bottom interface (negative voltage), the oxygen gas bubbles are stored at the bottom interface of the device, generating a large amount of damage in the active layer.

Aluminium oxide layers deposited by several techniques, such as anodization,<sup>2</sup> atomic layer deposition<sup>14,15</sup> and sputtering,<sup>16</sup> have shown rewritable memory behaviour in MIM devices. However, only a few reports of memory behaviour involving the native aluminium oxide film have been reported<sup>17,18</sup>. One of these reports<sup>17</sup> showed that the resistive switching in their aluminium/organic/metal devices is mainly caused by the formation of a thin native oxide layer. By using thermal images obtained with a CCD camera, they proved that the resistive switching observed in their devices was caused by the creation and destruction of filaments in the native AlOx layer. On the other hand, organic polymers have been used as the active layer in memory devices due to their excellent properties such as flexibility and good processability.

Poly(3,4-ethylenedioxythiophene):poly(styrenesulfonate) (PEDOT:PSS) is one of the most widely used conductive polymers owing to its high conductivity, high visible light transmission, high stability and water solubility.<sup>19</sup> PEDOT:PSS films have shown rewritable memory behaviour when used as the active layer<sup>20,21</sup> or when mixed with carbon nanotubes.<sup>22</sup> In a previous report,<sup>23</sup> we fabricated a rewritable memory device using a mixture of PEDOT:PSS and nitrogen-doped multiwalled carbon nanotubes (N-MWCNTs) embedded between two aluminium electrodes. It was found that the presence of a native aluminium oxide layer at the bottom electrode was crucial for obtaining the rewritable memory behaviour. Moreover, optical photographs showed protrusions on the top electrodes of the rewritable memory devices due to the

<sup>a</sup> Advanced Materials Department, IPICYT, Camino a la Presa San José 2055, Col.

Lomas 4a sección, San Luis Potosí 78216, Mexico. E-mail: sandov@ipicyt.edu.mx

<sup>b</sup> Instituto de Investigación en Comunicación Óptica, Universidad Autónoma de San Luis Potosí, Álvaro Obregón 64, San Luis Potosí 78000, Mexico. E-mail: reyesm@iico.uaslp.mx

Electronic Supplementary Information (ESI) available:

## ARTICLE

application of voltage pulses. This indicates that electrochemical processes occur in the native oxide layer during device electroforming and play a key role in the memory behaviour.

In this work, we fabricated an Al/PEDOT:PSS+N-MWCNTs/Al memory device. The devices were programmed to the ON state with the negative bias voltage and to the OFF state with the positive bias voltage. The devices showed a current-controlled rewritable memory only if a minimum compliance current (CC) was applied during the electroforming process, ranging from  $CC \sim 5$  mA to  $\sim 10$  mA for positive and negative voltages. The memory devices showed the presence of spherical deformations on the top electrode for positive and negative voltages. Using atomic force microscopy (AFM) and scanning electron microscopy (SEM), these spherical deformations were studied in order to elucidate the mechanism of the resistive switching. The novelty of the present work relies mainly in (a) the formation of oxygen gas bubbles in native aluminium oxide films, similar to those reported in well-studied  $\text{TiO}_2$ -based resistive memory devices, and (b) the memory devices being current-controlled, implying that a minimum CC is necessary during the electroformation process in order to obtain the resistive switching. The application of a higher bias voltage does not give rise to resistive switching if this minimum CC is not reached.

## B. Experiment

PEDOT:PSS (Clevios P), was purchased from Heraeus, whereas N-MWCNTs were synthesized by the spray pyrolysis method using a mix of ethanol and benzylamine (9:1 v/v) as the carbon, nitrogen and oxygen source, with ferrocene as a catalyst.<sup>24-26</sup> Prior to the deposition of the Al bottom electrode, 1-in<sup>2</sup> Dow Corning glass substrates were cleaned by washing in acetone, methanol and isopropanol in ultrasonic baths for 20 min and then dried for 40 min. Then, a 70 nm Al bottom electrode was deposited by thermal evaporation at  $10^{-6}$  Torr and patterned using a shadow mask. The nitrogen-doped carbon nanotubes and PEDOT:PSS composites were prepared by using the following procedure: the carbon nanotubes were dissolved in isopropanol, and the dispersion was ultrasonicated for 40 min at 58 °C. Then, 0.002 wt% of N-MWCNTs was mixed with a PEDOT:PSS aqueous solution for 150 min by ultrasonication at room temperature. This composite was spin-coated at 2500 rpm for 40 seconds onto the Al bottom electrode and then dried at 100 °C for 15 min. The PEDOT:PSS+ N-MWCNT film thickness was measured using a Tencor Alpha-Step 500 surface profiler and was found to be approximately 80 nm. Finally, a thermally evaporated 70 nm top electrode was deposited onto the polymeric composite layer and patterned using a shadow mask. The active area of the devices corresponds to the overlapping area between the bottom and top electrodes, which was 6 mm<sup>2</sup>. Current-voltage measurements were performed using a programmable Keithley 236 source meter at room conditions. In all current-voltage measurements of the memory devices, the bias voltage was applied to the top electrode with the grounded bottom electrode. Morphological characterizations of the rewritable memory devices were performed using a Quanta 250 scanning electron microscope operated at 20 kV and a Jeol JSPM-5200 atomic force microscope in the contact mode. AFM images were processed using WSMX software.<sup>27</sup>

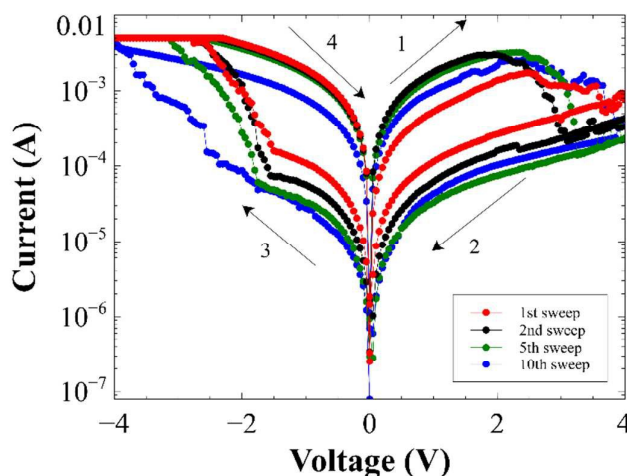


**Fig. 1** I-V characteristics of the Al/PEDOT:PSS+N-MWCNTs/Al device. Voltage sweeps from 0 to 4 V, from -4 to 4 V and from 4 to 0 V were applied 10 times to the pristine device with the compliance current of 5 mA.

## C. Results and discussions

Al/PEDOT:PSS+N-MWCNTs/Al devices can be electroformed to the ON state using positive bias or to the OFF state using negative bias.<sup>23</sup> After electroforming, the subsequent voltage sweeps are identical either if we start with negative or positive bias, in agreement with inorganic resistive memory devices based on  $\text{TiO}_2$ .<sup>12</sup> These Al/PEDOT:PSS+N-MWCNTs/Al devices switch from the ON to the OFF state at  $\sim 3$  V and from the OFF to the ON state at  $\sim -2$  V. Figure 1 shows the I-V characteristics for the first 10 switching curves on the semi-logarithmic scale using the compliance current of 5 mA. The memory devices display an ON-OFF ratio of  $10^3$  and more than 500 write-read-erase-read (WRER) cycles, as shown in our previous report.<sup>23</sup> Additionally, they exhibited deformations on the top electrode in the form of bubbles and showed rewritable behaviour only when the aluminium was used as the bottom electrode, instead of gold which is a material difficult to oxidize. Thus, this I-V behaviour is due to the presence of a native aluminium oxide thin film on the bottom electrode as well as the formation of these bubbles during the electroforming process.<sup>23</sup>

To elucidate whether the origin of the resistive switching of the rewritable memory behaviour in our devices is similar to that reported for the Pt/ $\text{TiO}_2$ /Pt memory device,<sup>12</sup> we study the morphological and physical properties of the deformations in the Al/PEDOT:PSS+N-MWCNTs/Al devices when positive or negative voltage pulses are applied to the pristine device. This enables a comparison of the resistive switching mechanisms between both kinds of devices; here, Al reacts with oxygen, creating a metal oxide phase, whereas Pt is a noble metal, and the oxygen can be reincorporated into the active layer of the memory device via electrochemical reactions. When a 4 V pulse with a duration of 2 seconds with  $CC=5$  mA is applied to the pristine device, spherical deformations are observed on the top electrode using SEM micrographs (Figure 2a), indicating the electroformation of the memory devices. After the voltage pulse application, the device is programmed to the OFF state. On the other hand, if a 4 V voltage

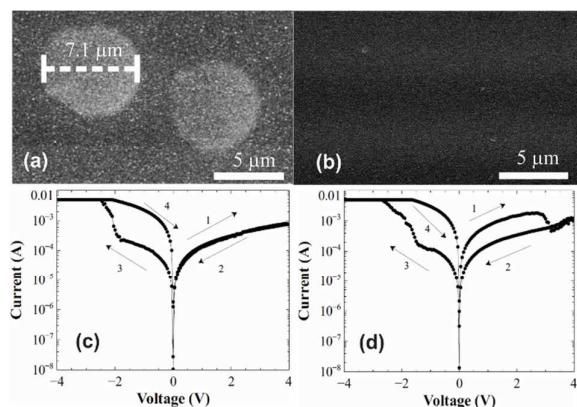


**Fig. 2** a) SEM micrograph of the top interface of the memory device shows bubbles owing to the application of a 4-V pulse with the compliance current of 5 mA. b) SEM micrograph of the top interface of the memory device after the application of a 4 V pulse with CC = 1 mA. No bubbles were observed. c) I-V curve of the memory device after the application of a 4 V pulse with CC= 5 mA. The device starts in the OFF state. d) I-V curve of the memory device after a 4-V pulse with CC= 1 mA was applied that not generated bubbles. The device starts in the ON state.

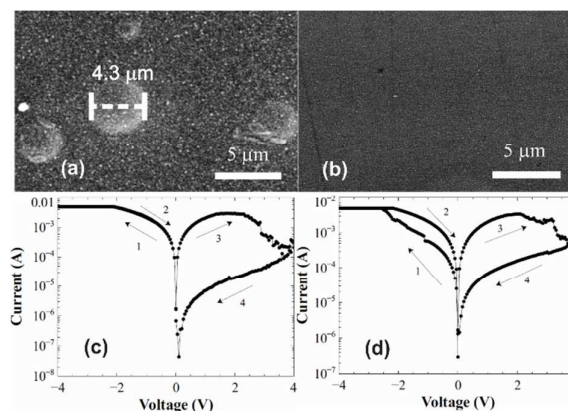


**Fig. 3** a) SEM micrograph of the top interface of the memory device show bubbles owing to the application of a -4 V pulse with the compliance current of 10 mA. b) SEM micrograph of the top interface of the memory device after the application of a -4 V pulse with CC= 1 mA. No bubbles were observed. c) I-V curve of the memory device after the application of a -4 V pulse with CC= 10 mA. The device starts in the ON state. d) I-V curve of the memory device after a -4 V pulse with CC= 1 mA that did not generate the bubbles was applied. The device starts in the OFF state.

pulse with a duration of 2 seconds and with CC = 1 mA is applied to the pristine device, neither memory behaviour nor deformations are observed (Fig. 2b). Moreover, device electroformation can be performed using voltage sweeps. For this purpose, a voltage sweep from 0 to 4 V, then from 4 to -4 V and finally from -4 to 4 V with the CC = 5 mA is applied to the device after: the application of a 4 V pulse for 2 seconds with CC = 5 mA (electroformed, shows in Figure 2a) or the application of 4 V pulse for 2 seconds with CC=1 mA (not electroformed, shows in Figure 2b). I-V curves of these devices after the application of the voltage sweeps (Figures 2c and 2d) show that the device without spherical deformations (Figure 2b) is electroformed when the voltage sweep is performed using a CC=5 mA. An examination of the figure shows that in the initial sweep from 0 to 4 V, the device with bubble formation (Figure 2c) remains in its OFF state, contrary to the device with no bubble formation (Figure 2d), which starts in the ON state and is electroformed to the OFF state at  $\sim 3$  V. Based on this result, it is deduced that the appearance of spherical deformation in the memory device is necessary for its electroformation and that the electroforming can be performed using voltage sweeps as long as the minimum CC is reached.

On the other hand, when a -4 V pulse with a duration of 2 seconds with CC = 10 mA is applied to a pristine device, spherical deformations of a smaller diameter are observed in the SEM micrographs (Figure 3a). Generally, a slightly higher CC is necessary to obtain electroforming in the ON state compared to electroformation in the OFF state, where CC=5 mA is sufficient. After the application of the voltage pulse, the device is programmed to the ON state. Similar to the device with the initial positive pulse, a minimal CC is necessary and sufficient to program the device. However, if a -4 V pulse with a duration of 2 seconds and CC = 1 mA is applied, the device is not programmed to the ON state, and spherical deformations are not observed (Figure 3b). I-V characterization of the devices is also performed using voltage sweeps from 0 to -4 V, from -4 to 4 V and finally from 4 to 0 V with CC = 5 mA after: the application of a -4 V pulse for 2 seconds with CC = 10 mA (electroformed, shows in Figure 3a) or the application of a -4 V pulse for 2 seconds with CC = 1 mA (not electroformed,

shows in Figure 3b). The device showing the bubbles started in the ON state (Figure 3c), while the device not showing bubbles started in the OFF state (Figure 3d); similar to the pristine devices, this device was electroformed to the ON state at -2 V.

Additionally, differences in the bubble sizes using both voltage polarities are observed using AFM. AFM micrographs show that the spherical deformations formed on the top electrode by the positive pulse (4 V for 2 sec and CC = 10 mA) have a diameter of  $\sim 7$  micrometres and a height of  $\sim 550$  nm (Figures 4a and 4b), while the bubbles formed on the top electrode by the negative pulse (-4 V for 2 sec and CC= 10 mA) show a smaller diameter ( $\sim 3$  micrometres) and a height of  $\sim 550$  nm (Figures 4c and 4d). On the other hand, if the I-V characterization of the pristine device is performed using voltage sweeps either starting at positive or negative voltages and with the CC below the minimum or threshold current, nonspherical deformations are generated, no memory behaviour is obtained, and the I-V curves of these devices exhibit an ohmic behaviour. Figure 5 shows this type of I-V behaviour, where voltage sweeps from 0 to 20 V, from 20 to -20 V and from -20 to 0 V with CC = 1 mA are applied. An examination of the figure shows that the device does not exhibit a resistive switching probably due to Joule heating requirement is not reached or there is not the critical energy for inducing the electroformation.<sup>28,29</sup> To observe the physical and morphological changes at the PEDOT:PSS+N-MWCNTs/Al interface, the Al top electrode was delaminated using scotch tape. SEM images are obtained on the top of the PEDOT:PSS+N-MWCNTs film after the application of positive (Figure 6a) and negative (Figure 6b) voltage pulses. For the devices electroformed with a positive polarity, no deformations are observed in the polymeric film, in contrast with the devices electroformed with a negative polarity, where circular craters are observed. This indicates that when a positive voltage is applied to the device, protrusions arise from the physicochemical phenomena occurring at the polymer/top electrode interface, whereas when a negative pulse is applied, the physicochemical phenomena occur at the polymer/bottom electrode interface, causing deformations in the polymer film. These protrusions are similar to those found for the Pt/TiO<sub>2</sub>/Pt

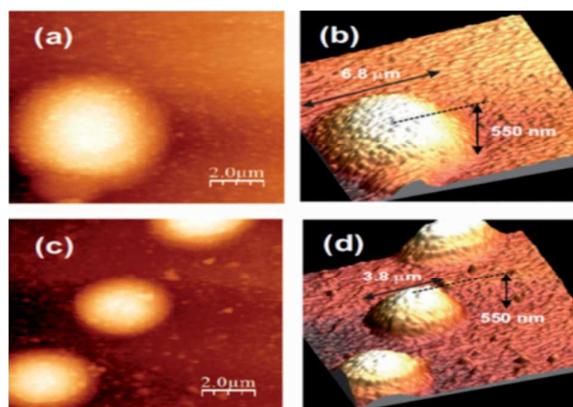


**Fig. 4** 2D (a) and 3D (b) AFM micrographs of the top interface after the application of a pulse of 4 V with CC= 10 mA. 2D (c) and 3D (d) AFM micrographs of the top interface after the application of a pulse of -4 V with CC= 10 mA.

devices<sup>12,13,30</sup> and have been related to the generation of oxygen vacancies in the TiO<sub>2</sub> film owing to redox reactions. The O<sup>2-</sup> ions are driven, accumulated, discharged, and then evolved as O<sub>2</sub> gas at the bottom electrode, showing a similar behaviour to that presented in this work. Thus, the dependence of bubble sizes observed on the Al top electrode as well as the damage occurring in the PEDOT:PSS + N-MWCNT active layer on the electroforming voltage polarity can be understood as follows: (a) when the electroforming polarity is positive, the top electrode corresponds to the device anode, and the oxygen ions are discharged on this and evolve as O<sub>2</sub> gas at the active layer/top electrode interface, giving rise to the delamination process of this electrode; (b) when the electroforming polarity is negative, the bottom electrode corresponds to the device anode, and the oxygen ions are discharged on this and evolve as O<sub>2</sub> gas at the bottom electrode/active layer interface; the O<sub>2</sub> gas accumulation at the bottom interface causes the delamination and

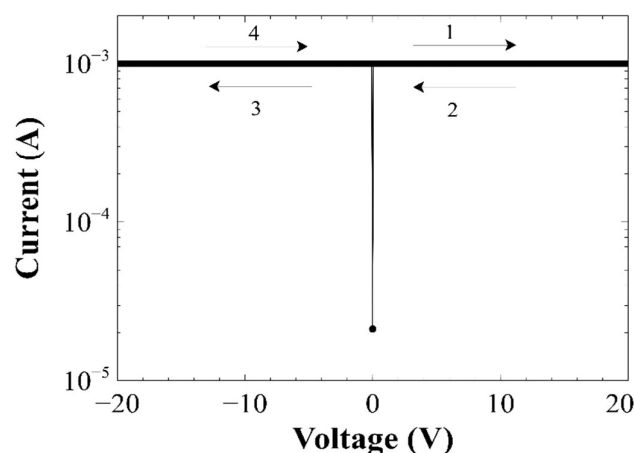


**Fig. 5** I-V curves of the memory device when sweeps from 0 to 20 V, from 20 to -20 V and from -20 to 0 V with CC= 1 mA are applied.

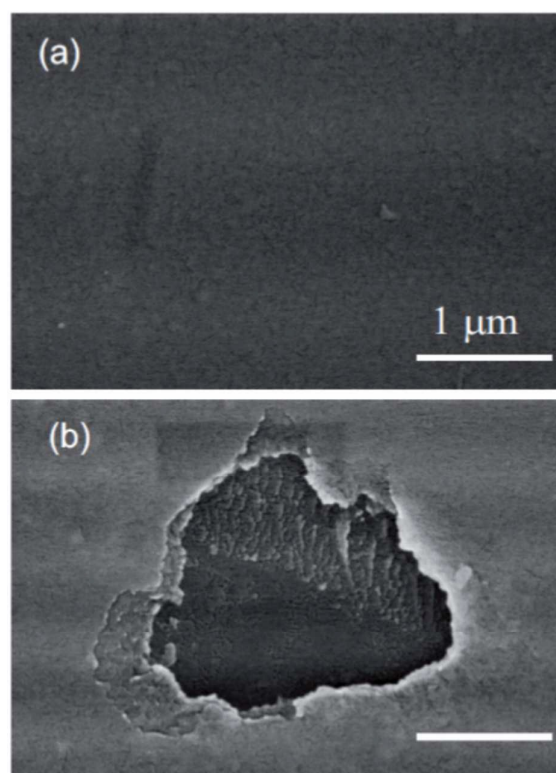


**Fig. 6** SEM micrographs on the top of the PEDOT:PSS+N-CNTs film after top electrode delamination after the application of: a) 4 V pulse with CC=10 mA and b) -4 V pulse with CC= 10 mA. Both scale bars are 1 micrometre.

damage of the active layer as well as a the smaller delamination of the top electrode. As discussed in the previous report, the creation/destruction of conductive filaments owing to the migration of oxygen vacancies through the PEDOT:PSS+N-MWCNTs active layer is unlikely to be the mechanism of resistive switching<sup>23,31</sup>, where the active layer and the native oxide film have thicknesses of ~80 nm and ~3 nm, respectively.<sup>32</sup> In our devices, the nitrogen-doped carbon nanotubes are necessary for obtaining the rewritable memory behaviour and act as conductive pathways.<sup>23</sup> This effect can be observed in Figure 7 and shows the polymeric film after the application of the -4 V pulse for 2 seconds with CC= 10 mA

. This figure presents a top view of the memory device after top electrode delamination showing several craters in the PEDOT:PSS+N-MWCNTs film in the vicinities of the carbon nanotubes. In the Pt/TiO<sub>2</sub>/Pt devices mentioned above,<sup>13,30</sup> the conductive paths are attributed to TiO<sub>2-x</sub> pillars formed in the centre of the craters in the TiO<sub>2</sub> film. These conductive paths are caused by the oxygen vacancy migration, i.e., electrochemical processes, and Joule heating crystallization of these TiO<sub>2-x</sub> pillars. In our devices, the results show that the carbon nanotubes near these craters play the role of conductive pathways, whereas the native aluminium oxide on the bottom electrode is the layer responsible for the resistive switching. Videos of optical images of the top electrode show bubble creation for both pulse polarities (4 V and -4 V) with CC= 10 mA (Videos S1 and S2, respectively). For both polarities, the

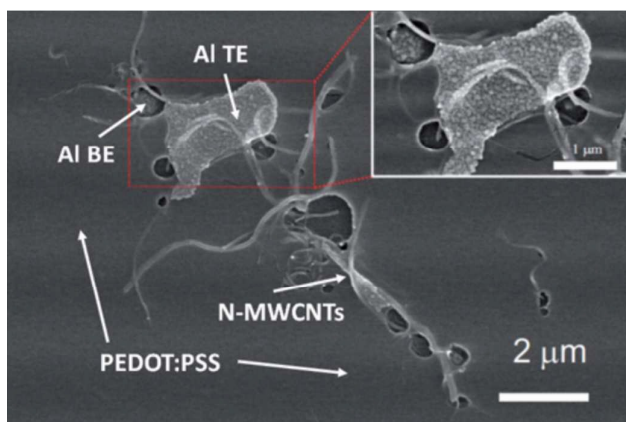


**Fig. 7** SEM micrograph of the memory device after the application of a -4 V pulse with CC= 10 mA. The top electrode was delaminated, leaving small islands of aluminium as can be observed. Circular craters induced by the negative voltage pulses are observed in the vicinity of the carbon nanotubes. Additionally, the bottom electrode can be observed through the hole formed in the polymeric film.

bubbles do not disappear when the voltage is turned off, contrary to the report by Yang et al.<sup>12</sup>, who reported that the bubbles on the top electrode disappear immediately after application of a positive voltage pulse for Pt/TiO<sub>2</sub>/Pt devices (Figure S1). This result could be related to the higher reduction potential of the aluminium compared to titanium. Moreover, it is known that the accumulation of the deformations causes the irreversible failure of the device.<sup>33</sup> Thus, further investigations are required for mitigating these deformations in the memory devices. Video S3 shows that when a positive voltage is applied, the device is electroformed, and bubbles are observed at the top electrode, whereas after the application of a negative voltage, the device does not show new deformations. The same phenomenon occurs when the application of a negative voltage is followed by the application of a positive voltage; only the first pulse application generates the spherical deformation (not shown), i.e., the device is electroformed in the first applied pulse or sweep, generating the oxygen vacancies in the devices. In addition, we have observed that the deformations in the memory devices can be diminished by exposing the top electrode to room conditions for 30 hours prior to the electrical measurements. SEM images show very small protrusions with diameters < 500 nm, and non-micron-sized bubbles are observed when voltage cycles are applied to the memory devices (Figure S2a) and the devices show rewritable memory behaviour (Figure S2b). This reduction of the deformations on the top electrode is related to the increase of the resistance of the aluminium layer after 30 hours of ambient exposure.

## D. Conclusions

In conclusion, spherical deformations are observed on the aluminium top electrode due to a redox process occurring in the native aluminium oxide films. Only the devices that exhibit deformations on the top electrode show resistive switching. These deformations are related to the creation of oxygen vacancies, and to the best of our knowledge, this is the first time that these deformations have been reported and studied in the native

aluminium oxide layer. The Al/PEDOT:PSS+N-MWCNTs/Al devices can be electroformed to the ON (OFF) state by the application of a negative (positive) voltage sweep or pulse. We have observed that the electroformation process is current-controlled; it is necessary to apply a voltage pulse or sweep with the compliance current greater than the threshold value that is generally between 5 and 10 mA in order to obtain a device showing resistive switching. SEM images of an electroformed device with a negative voltage after top electrode delamination show a large number of craters in the vicinity of the carbon nanotubes, suggesting that these play the role of conductive pathways, similar to the TiO<sub>2-x</sub> conductive pillars reported in Pt/TiO<sub>2</sub>/PT memory devices.

## Acknowledgements

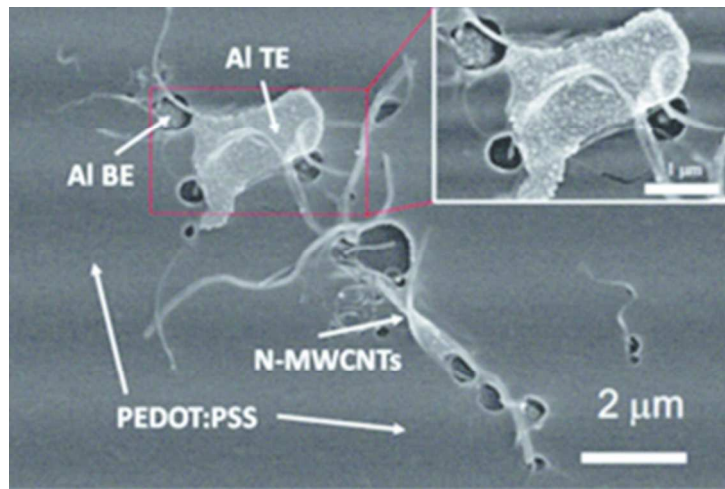
The authors acknowledge Francisco Ramírez Jacobo, M. Sc. Dulce Partida-Gutierrez, M. Sc. Beatriz A. Rivera, M. Sc. Ana I. Peña, Dr. Gladis Labrada and Dr. Hector G. Silva-Pereyra for technical assistance as well as to LINAN at IPICYT for providing access to its facilities. X-ray photoelectron spectra were obtained by Dr. Mariela Bravo-Sanchez at LINAN-IPICYT. This work was supported by CONACYT through grant No. CB-2015-01-256484 (R.L.S) J.A.A.N. thanks to the Fondo Sectorial-CONACYT-SENER-Hidrocarburos for a posdoctoral grant (2137).

## References

- 1 A. Sawa, *Mater. Today*, 2008, **11**, 28.
- 2 T.W. Hickmott, *J. Appl. Phys.*, 1962, **33**, 2669.
- 3 A. Beck, J. G. Bednorz, Ch. Gerber, C. Rossel and D. Widmer, *Appl. Phys. Lett.*, 2000, **77**, 139.
- 4 D.S. Jeong, R. Thomas, R. S. Katiyar, J. F. Scott, H. Kohlstedt, A. Petraru and C. S. Hwang, *Rep. Prog. Phys.*, 2012, **75**, 076502.
- 5 L.W. Feng, C.Y. Chang, Y.F. Chang, W.R. Chen, S.Y. Wang, P.W. Chiang and T.C. Chang, *Appl. Phys. Lett.*, 2010, **96**, 052111.
- 6 Y.F. Chang, T.C. Chang and C.Y. Chang, *J. Appl. Phys.*, 2011, **110**, 053703.
- 7 L.W. Feng, C.Y. Chang, Y.F. Chang, T.C. Chang, S.Y. Wang, S.C. Chen, C.C. Lin, S.C. Chen and P.W. Chiang, *Appl. Phys. Lett.*, 2010, **96**, 222108.
- 8 W.P. Lin, S.J. Liu, T. Gong, Q. Zhao and W. Huang, *Adv. Mater.*, 2014, **26**, 570.
- 9 B. Cho, S. Song, Y. Ji, T.W. Kim and T. Lee, *Adv. Funct. Mater.*, 2011, **21**, 2806.
- 10 L.W. Feng, Y.F. Chang, C.Y. Chang, T. Chang, S.Y. Wang, P.W. Chiang, C.C. Lin, S.C. Chen and S.C. Chen, *Thin Solid Films*, 2010, **519**, 1536.
- 11 M. Q. Guo, Y.C. Chen, C.Y. Lin, Y.F. Chang, B. Fowler, Q. Q. Li, J. Lee and Y.G. Zhao, *Appl. Phys. Lett.*, 2017, **110**, 233504.
- 12 J. J. Yang, F. Miao, M. D. Pickett, D. A. A. Ohlberg, D. R. Stewart, C. N. Lau and R. S. Williams, *Nanotechnology*, 2009, **20**, 215201.
- 13 R. Münstermann, J. J. Yang, J. P. Strachan, G. Medeiros-Ribeiro, R. Dittmann and R. Waser, *Phys. Status Solidi RRL*, 2010, **4**, 16.
- 14 K. Park and J.S. Lee, *RSC Adv.*, 2016, **62**, 1736.

- 15 Y.C. Chen, Y.F. Chang, X. Wu, F. Zhou, M. Guo, C.Y. Lin, C.C. Hsieh, B. Fowler, T.C. Chang and J.C. Lee, *RSC Adv.*, 2017, **7**, 12984
- 16 F. Verbakel, S. C. J. Meskers, R. A. J. Janssen, H. L. Gomes, M. Cölle, M. Büchel and D. M. de Leeuw, *Appl. Phys. Lett.*, 2007, **91**, 192103.
- 17 M. Cölle, M. Büchel, and D. M. de Leeuw, *Org. Electron.*, 2006, **7**, 305.
- 18 S. Karthäuser, B. Lüssem and M. Weides, *J. Appl. Phys.*, 2006, **100**, 094504.
- 19 L. Groenendaal, F. Jonas, D. Freitag, H. Pielartzik and J. R. Reynolds, *Adv. Mater.*, 2000, **12**, 481.
- 20 H. Ha and O. Kim, *Appl. Phys. Lett.*, 2008, **93**, 033309.
- 21 X. Liu, Z. Ji, D. Tu, L. Shang, J. Liu, M. Liu and C. Xie, *Org. Electron.*, 2009, **10**, 1191.
- 22 J. A. Avila-Niño, W. S. Machado, A. O. Sustaita, E. Segura-Cardenas, M. Reyes-Reyes, R. López-Sandoval and I. A. Hümmelgen, *Org. Electron.*, 2012, **13**, 2582.
- 23 I. Rosales-Gallegos, J.A. Avila-Niño, D. Hernández-Arriaga, M. Reyes-Reyes and R. López-Sandoval, *Org. Electron.*, 2017, **45**, 159
- 24 A. Antal, A.A. Koos, F. Dillon, R.J. Nicholls, L. Bulusheva and N. Grobert, *Chem. Phys. Lett.*, 2012, **538**, 108.
- 25 E. Segura-Cardenas, M. Reyes-Reyes and R. Lopez-Sandoval, *J. Phys. Chem. C*, 2012, **116** (17), 9783.
- 26 E. Segura-Cardenas, R. Lopez-Sandoval, D. Hernandez-Arriaga, J. Percino, V.M. Chapela and M. Reyes-Reyes, *Carbon*, 2014, **76**, 292.
- 27 I. Horcas, R. Fernandez, J. Gomez-Rodriguez, J. Colchero, J. Gomez-Herrero and A.M. Baro, *Rev. Sci. Instrumen.*, 2007, **78**, 013705.
- 28 K.C. Chang, T.C. Chang, T.M. Tsai, R. Zhang, Y.C. Hung, Y.E. Syu, Y.F. Chang, M.C. Chen, T.J. Chu, H.L. Chen, C.H. Pan, C.C. Shih, J.C. Zheng and S.M. Sze, *Nanoscale Res. Lett.*, 2015, **10**, 120.
- 29 F. Zhou, Y.F. Chang, Y.C. Chen, X. Wu, Y. Zhang, B. Fowler and J.C. Lee, *Phys. Chem. Chem. Phys.*, 2016, **18**, 700.
- 30 J.P. Strachan, J. J. Yang, R. Münstermann, A. Scholl, G. Medeiros-Ribeiro, D. R. Stewart and R. S. Williams, *Nanotechnology*, 2009, **20**, 485701.
- 31 S. Nigo, M. Kubota, Y. Harada, T. Hirayama, S. Kato, H. Kitazawa and G. Kido, *J. Appl. Phys.*, 2012, **112**, 033711.
- 32 I.A. Rosales-Gallegos, J.A. Avila-Niño, M. Reyes-Reyes, O-Núñez-Olvera and R. López-Sandoval, *Thin Solid Films*, 2016, **619**, 10.
- 33 M. Trapatseli, D. Carta, A. Regoutz, A. Khiat, A. Serb, I. Gupta and T. Prodromakis, *J. Phys. Chem. C*, 2015, **119**, 11958.

Physical deformations in organic resistive memories coming from redox processes occurring in the native aluminium oxide layer due to electroformation.



30x20mm (300 x 300 DPI)